ACS OMEGA

http://pubs.acs.org/journal/acsodf

Article

Flame Propagation Characteristics of Syngas-Air in the Hele-Shaw Duct with Different Equivalence Ratios and Ignition Positions

Shoutong Diao, Xiaoping Wen,* Zhidong Guo, Wenqiang He, Haoxin Deng, and Fahui Wang

Cite This: *ACS Omega* 2022, 7, 20118−20128

Read Online

ACCESS | Metrics & More | Article Recommendations

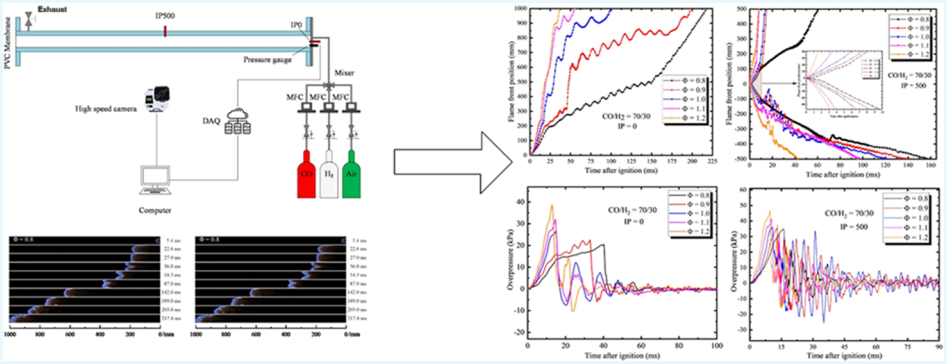

ABSTRACT: In this paper, the effects of different ignition positions and equivalence ratios on the explosion characteristics of syngas in a half-open Hele-Shaw duct were investigated. The ignition points are set at distances of 0 and 500 mm from the closed end. Moreover, the research range of equivalence ratio is 0.8−1.2. The experimental results indicate that different ignition positions and equivalence ratios influence the flame front structure and the dynamic characteristics of flame propagation. When the ignition position is at the closed end, the flame front undergoes several typical propagation stages before eventually reaching the open end of the duct. The time required by the flame to reach the open end decreases as the equivalence ratio increases. Meanwhile, when the ignition is in the middle of the duct, the flame simultaneously spreads to the open and closed ends. The time required to reach both sides decreases with the increase in the equivalence ratio. The flame front structure and pressure are primarily affected by the ignition position and the equivalence ratio. At the same ignition position, flame propagation velocity and maximum overpressure increase with the equivalence ratio. The pressure oscillation becomes more intense when the ignition position is close to the open end. At IP_{500}, when the equivalence ratio is 0.8, multiple finger-shaped flame fronts emerge, accompanied by high-frequency flame oscillations. This study can provide guidance for the study of the flame propagation characteristics of syngas in millimeter-scale burners.

1. INTRODUCTION

Carbon monoxide is a colorless and odorless gas. When the human body inhales higher concentrations of carbon monoxide, it causes strong toxicity.[1,2] In addition, due to the presence of hydrogen, the ignition energy of the synthesis gas is low, and the flammable limit is wide.[3] In the process of storage, transportation, and use of syngas, an explosion is a potential hazard that can cause personal injury and damage to the surrounding environment. Therefore, understanding the explosive characteristics of syngas is crucial for its safe use.

In recent years, many researchers have conducted experimental and numerical studies on the explosive characteristics of syngas. Yu et al.[4,5] studied the effect of ignition position and hydrogen concentration on the flame propagation characteristic of syngas in a rectangular tube and found that flame propagation velocity increases with the increase in hydrogen concentration. The pressure oscillation becomes more intense when the ignition position is far from the closed end. Also, the flame behavior in the closed duct is different than that in the half-open duct. The opening duct has a faster flame propagation speed and lowers the overpressure. Guo et al.[6] used experimentally different opening ratios and hydrogen volume fractions of syngas in a cylindrical combustion duct. Their experimental results show that the increase in the pressure amplitude is closely related to the change in the opening ratio and the hydrogen volume fraction. Wen et al.[7]

Received: March 31, 2022
Accepted: May 24, 2022
Published: June 3, 2022

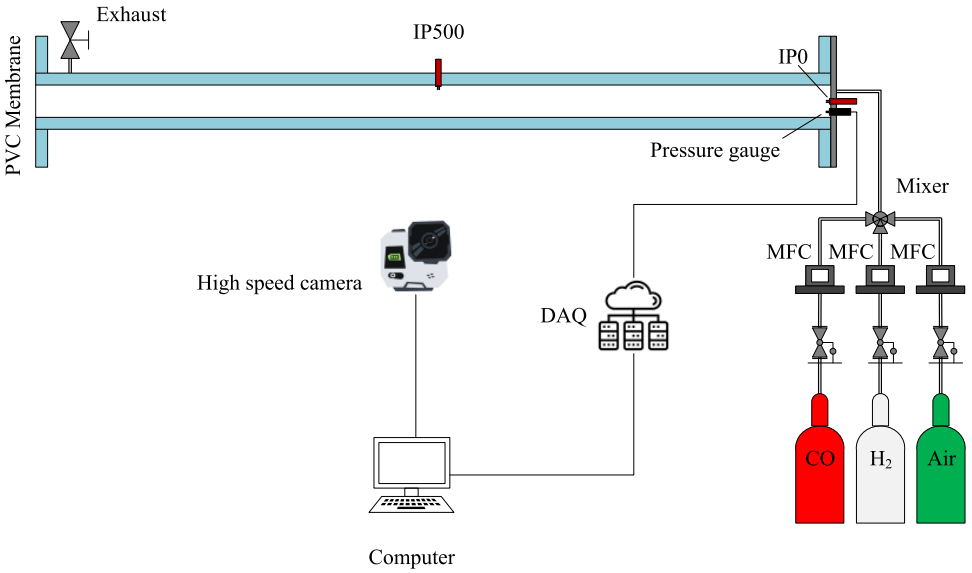

Figure 1. Schematic diagram of the experimental setup.

also analyzed the opening ratio and the ignition position of syngas in a rectangular duct. Sun[8] and Singh et al.[9] conducted experimental work to measure the laminar flame speed and explosion overpressure of premixed syngas/air mixtures in the spherical combustion. Zheng et al.[10] experimentally studied the explosion behavior of syngas/air mixture under the effect of N_2 and CO_2 additions. The experimental results show that CO_2 is more effective than N_2 in terms of flame velocity and overpressure. Luo et al.[11,12] also performed many research studies in the field of gas explosion. They[11] conducted an experimental study on the explosion characteristics of CH_4/H_2 mixed fuel under nitrogen dilution conditions. Furthermore, the effects of ferromagnetic metal velvet and DC magnetic field on explosion were studied for the C_3H_8/air mixture.[12]

A Hele-Shaw duct is an area between closely spaced plane-parallel plates. This setup was initially used by Hele-Shaw[13] and Saffman[14] to study the viscous effects on different fluids. It is of far-reaching significance to study the propagation characteristics of premixed flames in this area. Studying the propagation of premixed gas flame in the Hele-Shaw duct can help the safe use of fuel cells and internal combustion engines.[15] Kurdyumov,[16] Fernando,[17] and Wongwiwat et al.[18] experimentally and computationally analyzed the hydrocarbon flame propagation in the Hele-Shaw duct. Also, they found a very interesting oscillation phenomenon of the flame. Jang et al.[19−21] used a narrow-gap disk burner to study the radial propagation characteristics of flame. In addition, Jiang et al.[22−24] conducted extensive studies on the flame propagation characteristics within a narrow-gap disk burner. They[22] experimentally investigated the effect of gap width and equivalence ratio on the propane−air flame propagation characteristics. The change in the flame front from smooth to wrinkled was observed, and the flame propagation velocity also decreased with the increase in the flame radius. In addition, they[24] also conducted an experimental study on the effect of different initial pressures on the flame propagation characteristics. The results showed that an increase in the initial pressure significantly increased the flame propagation velocity and the pressure peak.

Although many scholars have carried out the combustion characteristics of syngas widely, most of the experiments and theoretical and numerical studies found in the literature have focused their attention on flame propagation in a rectangular, cylindrical, or spherical duct. The purpose of this study is to investigate the explosion characteristic of syngas/air mixture in the Hele-Shaw duct. In this experiment, five cases of equivalence ratios and two cases of ignition positions were studied. Flame images and explosion overpressure are recorded by high-speed cameras and pressure sensors. Also, this work may provide a basis for the safe utilization of syngas in the manufacturing process.

2. EXPERIMENTAL SECTION

This experiment uses the previously built narrow channel experimental platform.[25,26] The experimental device is shown in Figure 1. It consists of the Hele-Shaw duct, the gas distribution system, the ignition system, the pressure acquisition system, and the image acquisition system. To realize the visualization during the experiment, the wall of the duct is made of plexiglass with a thickness of 20 mm. The size of the combustion duct is 1000 mm × 50 mm × 10 mm. In the experiment, a TP304 stainless steel plate is used to seal the right side of the duct and a poly(vinyl chloride) (PVC) is used to seal the other side. The left end of the duct can be regarded as a pressure relief outlet. The flow of gases used in the experiment is controlled using the mass flow controller. Gas in the high-pressure cylinder enters the mass flow controller after decompression through a pressure relief valve. Then, the gas in the mixer is premixed into the experimental duct. The premixed gas enters the duct through the air inlet hole at the sealed end and can be discharged through the valve on the duct wall near the exhaust end. To ensure that the original air in the duct is completely discharged, at least four times the volume of the gas premixed in the duct should be introduced.[27] The pressure generated by the explosion is collected by a pressure sensor at a frequency of 200 kHz. The image acquisition system includes a high-speed camera and PCC computer software. High-speed cameras are used to capture dynamic images of the flame propagation process. Also, the sampling frequency is 3000 frame/s.

During the processing of the pressure signal, the pressure curve is smoothly processed using the Origin software. We use

https://doi.org/10.1021/acsomega.2c01960
ACS Omega 2022, 7, 20118−20128

the FFT filtering method of the 10-point data window to smoothen the curve. The purpose is to eliminate the effects of interference signals on true pressure curves. Further, the collected pressure signals are partially deleted, and only the pressure data after the ignition is retained. The contrast of the processed pressure curve to the original curve is shown in Figure 2.

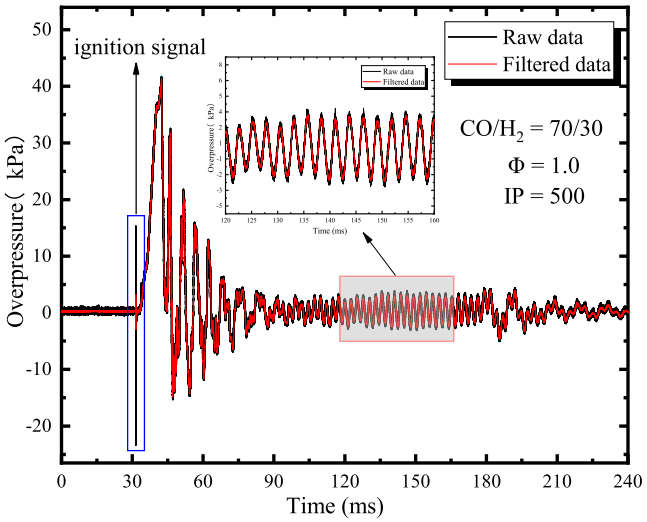

Figure 2. Pressure curve processing and smooth procedure.

This experimental setup has two different ignition positions, IP_0 (0 mm from ignition) and IP_{500} (500 mm from ignition). Five different equivalence ratios with 0.8, 0.9, 1.0, 1.1, and 1.2 are set, and the ratio of carbon monoxide to hydrogen is 7:3. The initial temperature T_0 of the experiment is 300 K, and the initial pressure P_0 is 101 kPa. To ensure the accuracy of the experiment, each set of working conditions is repeated at least three times. The exhaust method was used for gas distribution in the experiment. When the amount of premixed gas introduced into the duct reaches 5 times the volume of the duct, it can be guaranteed that the duct is filled with the premixed gas. The equivalence ratio, Φ, is defined as

$$\Phi = \frac{(A/F)_{\text{stoic}}}{A/F} = \frac{(m_{\text{air}}/m_{\text{fuel}})_{\text{stoic}}}{(m_{\text{air}}/m_{\text{fuel}})} \quad (1)$$

where m_{air} and m_{fuel} are the masses of the flow of air and syngas. $(A/F)_{\text{stoic}}$ is the air−fuel ratio under chemical equivalence.

3. RESULTS AND DISCUSSION

3.1. Flame Structure Evolution. Figures 3 and4 show the syngas/air explosion flame images at different equivalence ratios when the ignition positions are IP_0 and IP_{500}, respectively. For the ignition position IP_{500}, the flame fronts propagating to the open/left end are named LFF and those propagating to the closed/right end are named RFF. The corresponding time is marked on each flame picture, so as to understand the evolution law of the flame more clearly.

First, we focused on the flame characteristic of IP_0. After ignition at IP_0, the explosion flame propagation is from the close end to the open end. As the flame spreads, the flame changes different shapes. This paper uses Salamandra's[28] and Searby's[29] nomenclatures for tulip flames and four dynamic propagation stages according to the characteristics of flames on a two-dimensional plane. For example, as shown in Figure 3a, the experimental result shows that spherical flame (t = 5.4 ms), finger-shaped flame (t = 22.6 ms), and tulip flame (t = 36 ms) appear successively. During the "finger-shaped flame" and "tulip flame", there is a process of gradual flattening at the flame front. After the "tulip flame" (t > 36 ms), there is an obvious acceleration of the flame. The flame front velocity is described in Section 3.2 of the article.

The flame structure evolution is different at IP_{500}. Figure 4 shows the flame evolution process of different equivalence ratios at the IP_{500} position. The flame at the LFF end went out of the tube after a short period of time, and none of the flame fronts formed a tulip flame. As shown in Figure 4a, at an equivalence ratio of 0.8, the flame propagates simultaneously to the RFF and LFF ends after ignition. At the beginning of flame propagation (t < 44.6 ms), due to the restriction of the sidewall, the flame is ellipsoid and accompanied by a small amplitude of flame oscillation. When t > 44.6 ms, the flame shape changes obviously, showing multiple finger-shaped flame fronts with high-frequency flame oscillation, and the maximum oscillation amplitude can reach 21.32 mm. The oscillation frequencies on both sides of RFF and LFF are consistent, but the left flame propagates faster than the right flame (t = 60.9 ms). As shown in Figure 5, flame fronts with multiple fingers and high-frequency flame oscillations disappear with the increase in the equivalence ratio. The propagation of flame in Hele-Shaw duct should be consider the hydrodynamic, the diffusive−thermal and the thermoacoustic instabilities.

The diffusive−thermal instability is determined by the physical properties of gas fuels and mixtures, and its dominant role in flame propagation depends on the Lewis number. Syngas is composed of two different fuels. For multicomponent fuels, the Lewis number can be calculated according to the methods in the literature.[30−32] There is a basic formulation

$$\text{Le}_{\text{eff}} = \frac{\alpha_{\text{mix}}}{X_1 D_{1/N_2} + X_2 D_{2/N_2}} \quad (2)$$

where α_{mix} is the thermal diffusivity of the mixture and D_{i/N_2} is the mass diffusivity of the different fuels. This article uses Cesare's[33] calculation results on D_{i/N_2}. X_i is the molar fraction of different fuels. Also, the thermal diffusivity of the mixture is calculated by

$$\alpha_{\text{mix}} = \frac{\lambda_{\text{mix}}}{\rho_{\text{mix}} c_{\text{p,mix}}} \quad (3)$$

Thermal conductivity (λ_{mix}) and heat capacity ($c_{\text{p,mix}}$) for gas mixtures is obtained by

$$\lambda_{\text{mix}} = \frac{1}{2}\left(\sum_{i=1}^{N} X_i \lambda_i + 1/\sum_{i=1}^{N} \frac{X_i}{\lambda_i} \right) \quad (4)$$

$$c_{\text{p,mix}} = \sum_{i=1}^{N} Y_i c_{P,i} \quad (5)$$

where ρ_{mix} is the density of the gas mixture and Y_i is the mass fractions of different gases. λ_i and $c_{\text{p},i}$ are the heat capacity and thermal conductivity, respectively. Table 1 lists the physical parameters of the syngas/air mixture at different equivalence ratios. T_b, ρ_{mix}, and S_L are calculated using the reaction mechanism of the H_2/CO combustion by Davis.[34]

https://doi.org/10.1021/acsomega.2c01960
ACS Omega 2022, 7, 20118−20128

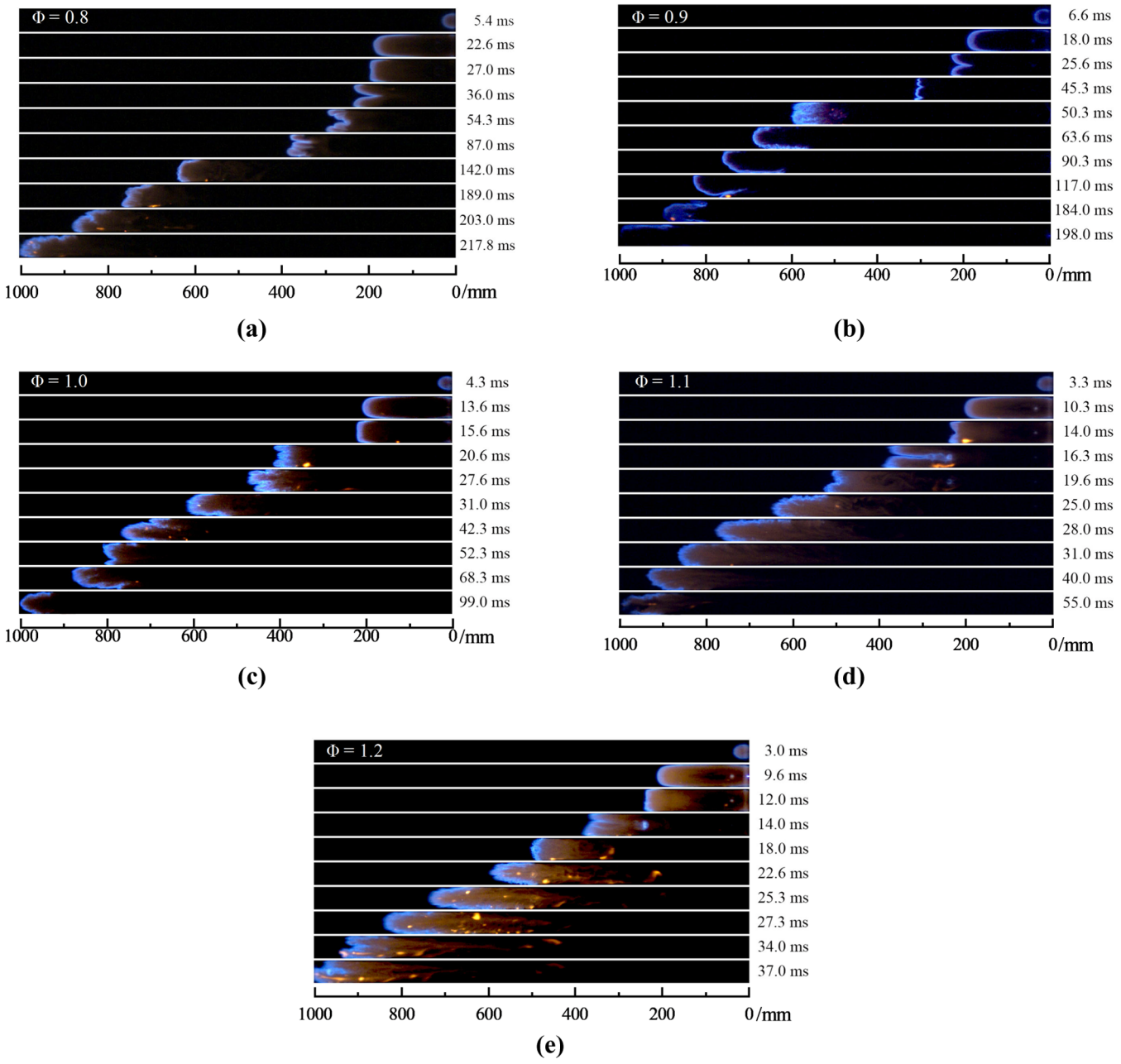

Figure 3. Flame dynamic images when ignited at IP_0: (a) Φ = 0.8, (b) Φ = 0.9, (c) Φ = 1.0, (d) Φ = 1.1, and (e) Φ = 1.2.

The competition between thermal diffusion and mass diffusion is one of the important sources of thermal diffusive instability. The importance of thermal diffusive instability in premixed flame propagation can be described by comparing the relative magnitude of thermal diffusivity and mass diffusivity, that is, the Lewis number. When Le < 1, thermal diffusive instability makes the flame front more unstable. However, Le > 1 is beneficial to stabilize the flame front.

In addition, hydrodynamic instability, one of the intrinsic instabilities of flame, is also a major factor affecting flame propagation. The hydrodynamic instability can be attributed to the difference in density before and after the flame front, which can be characterized by the thermal expansion ratio. The larger the thermal expansion ratio, the more likely it is for flame instability to be caused by hydrodynamic instability.

Thermoacoustic instability is caused by the coupling of heat produced by combustion chemical reactions with sound waves produced in a closed or half-closed duct. This instability at the flame front causes strong flame oscillation and seriously affects the stability of combustion. Considering the fuel mixtures with different ignition positions and components, the multiple finger flame fronts and strong flame oscillations under IP_{500} and Φ = 0.8 conditions are mainly caused by diffusive−thermal and thermoacoustic instability.

3.2. Flame Tip Characteristic. The flame position farthest from the ignition end is the flame front, determined as the distance from the flame front to the ignition electrode. Flame propagation velocity is calculated by dividing the propagation distance of the flame front into two consecutive images. The image processing function of MATLAB aims to obtain the flame front position.[26] First, it converts the image recorded by

https://doi.org/10.1021/acsomega.2c01960
ACS Omega 2022, 7, 20118−20128

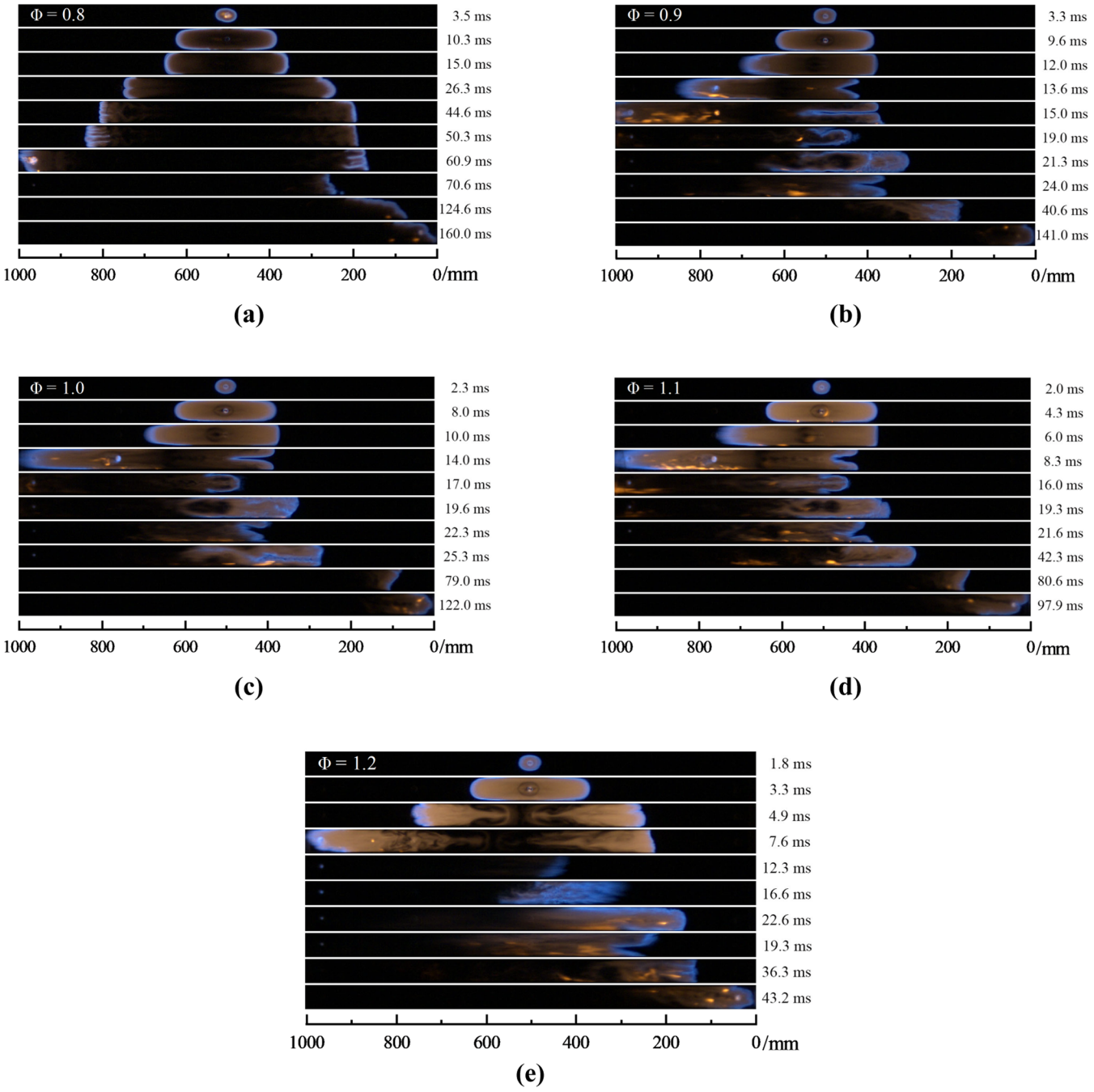

Figure 4. Flame dynamic images when ignited at IP_{500}: (a) Φ = 0.8, (b) Φ = 0.9, (c) Φ = 1.0, (d) Φ = 1.1, and (e) Φ = 1.2.

a high-speed camera into its grayscale counterpart. Then, the image is converted into a binary image according to the brightness threshold. From this binary image, the boundary of the flame front is obtained.

As indicated in Figure 5, there is a great correspondence between flame front position, flame velocity, and flame structure. The photographs of the flame structure corresponding to the flame velocity at a given time indicated in Figure 5a can be found in Figure 5b. In the spherical and finger flame stages, flame velocity increases linearly (A). Subsequently, the interaction between the sidewall and the flame surface causes the flame front to flatten to form a plane flame, while the corresponding flame velocity begins to decrease (B). Afterward, the flame front develops into a typical tulip flame (C) and a distorted tulip flame (D). When the PVC membrane at the LFF end ruptures, the pressure created by the release of gas in the duct causes a sudden acceleration of the flame (E). The flame then fluctuates periodically.

Figure 6 illustrates the flame front positions at different equivalence ratios with IP_0 and IP_{500}. Here, we define the time required for the flame to reach both ends of the combustion chamber at varying ignition positions and equivalence ratios. At IP_0, with the increase in the equivalence ratio, the time required by the flame to reach the LFF end gradually shortens. When Φ = 0.8, the time required by the flame to reach the LFF end is 217.8 ms; when it increases from 0.8 to 0.9 and 1.0, the time required by the flame to reach the end of the duct is 198 ms and 99 ms, while flame propagation time is shortened by

https://doi.org/10.1021/acsomega.2c01960
ACS Omega 2022, 7, 20118−20128

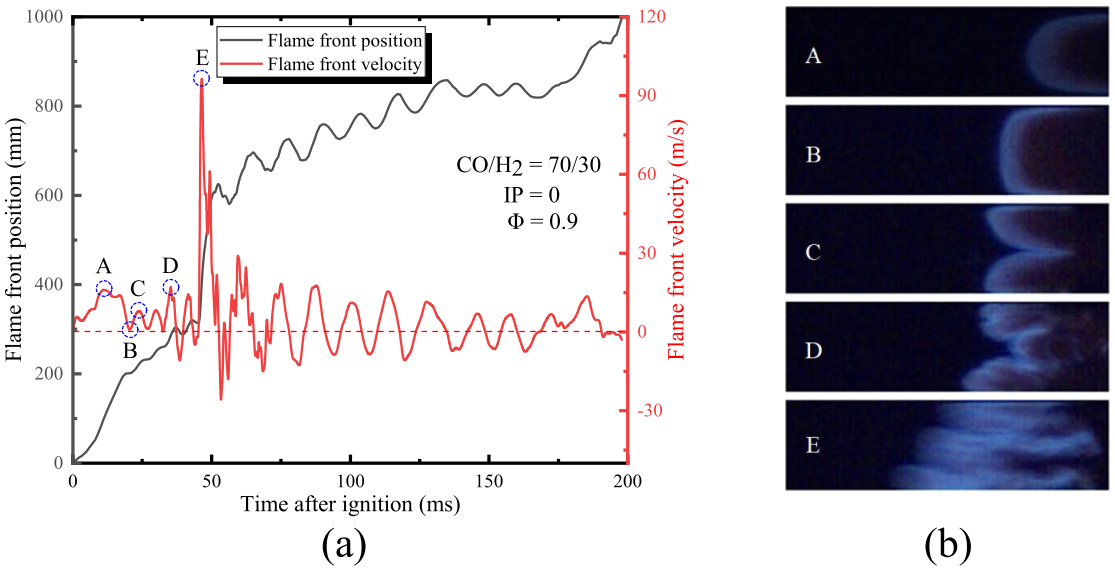

Figure 5. (a) Coupling relationship between flame propagation speed and flame front position of LFF. (b) Flame structural evolution of LFF (Φ = 0.9, IP = 500 mm).

Table 1. Properties of Syngas/Air Premixes at Different Equivalence Ratios

Φ	T_b [k]	S_L [cm/s]	ρ_{mix} [kg/m^3]	α_{mix} [m^2/s]	λ_{mix} [W/mk]	$c_{p,mix}$ [J/kgK]	Le_{eff}
0.8	2212	58.92	1.069	2.81×10^{-5}	3.28×10^{-2}	1091.45	0.75
0.9	2305	70.40	1.061	2.86×10^{-5}	3.34×10^{-2}	1099.43	0.77
1.0	2360	81.97	1.054	2.91×10^{-5}	3.40×10^{-2}	1107.04	1.42
1.1	2389	92.09	1.047	2.96×10^{-5}	3.45×10^{-2}	1114.31	1.44
1.2	2395	101.76	1.041	3.01×10^{-5}	3.51×10^{-2}	1121.26	1.47

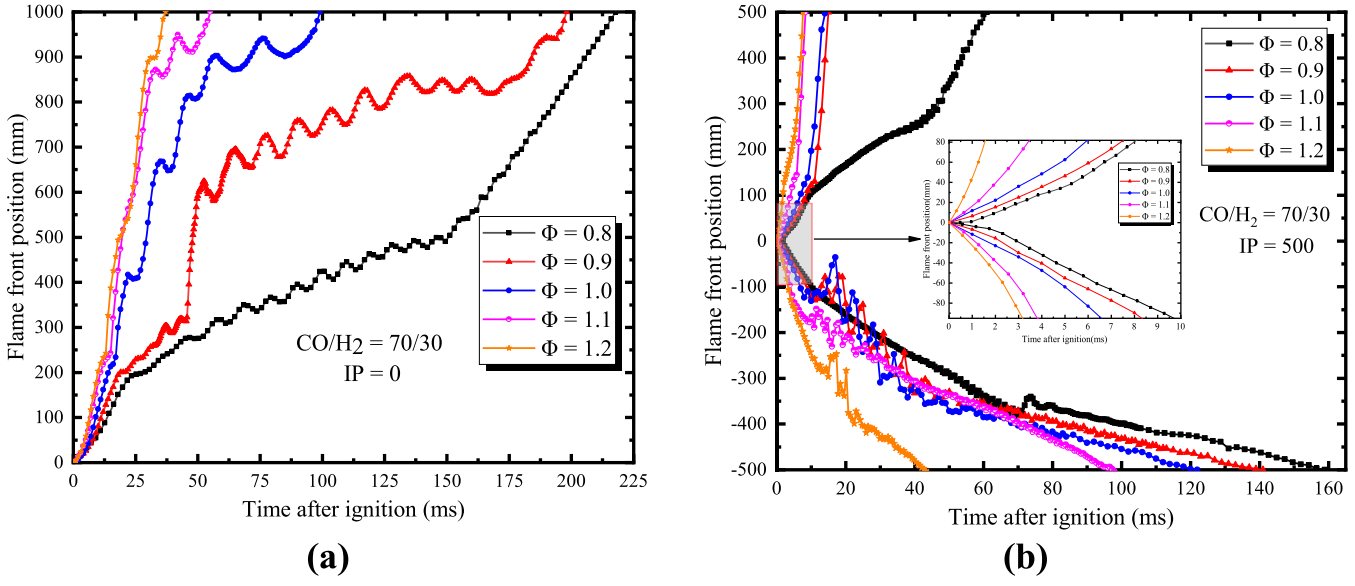

Figure 6. Position of the flame front: (a) IP_0 and (b) IP_{500}.

19.8 and 118.8 ms, respectively. As the equivalence ratio continues to increase to 1.0 and 1.2, the flame propagation time to reach the duct's end decrease to 55 and 37 ms, respectively. Different oscillation degrees accompany the flames during propagation, all appearing in the late stage of flame propagation. With the increase in equivalence ratio, the frequency of the flame oscillation decreases little by little.

Figure 6b provides the flame front position versus time for IP_{500} with Φ = 0.8, 0.9, 1.0, 1.1, and 1.2. Similar effects of equivalence ratios exist on flame fronts at IP_{500} and IP_0. With the increase in the equivalence ratio, the flames arrive at LFF and RFF earlier. From Table 2, when the equivalence ratio is in the range between 0.8 and 1.2, the times required by the flame to reach the LFF end are 60.9, 15, 14, 8.32, and 7.60 ms, respectively. Meanwhile, the respective times to reach RFF are 158.9, 141, 122, 97.9, and 43.2 ms. When the flame is near the exit at the LFF end, the flame front at the RFF end begins to reverse and then oscillates periodically due to the release of

https://doi.org/10.1021/acsomega.2c01960
ACS Omega 2022, 7, 20118−20128

Table 2. Time Required by the Flame to Reach the End of the Duct

	IP0		IP500	
equivalence ratio (Φ)	LFF	RFF (ms)	LFF (ms)	RFF (ms)
0.8		217.8	60.9	158.92
0.9		198.0	15.0	141.0
1.0		99.0	14.0	122.0
1.1		55.0	8.32	97.9
1.2		37.0	7.6	43.2

unburned gas and the cumulative pressure before the rupture of the PVC film. Thus, we can reasonably assume that the release of LFF flame is the primary reason for the periodic fluctuation of the RFF. When the combustion gas is released from the duct, the pressure inside the duct decreases sharply. Consequently, the released pressure inevitably has a strong pulling effect, causing the central part of the RFF end to reverse the propagation direction.

Thermoacoustic instability in the Hele-Shaw channels cannot be ignored due to space constraints, fundamentally caused by the coupling of the acoustic wave and flame. This phenomenon occurs in closed and semiclosed spaces. Velocity coupling occurs when the flame front interacts with the velocity field generated by the pressure, resulting in acceleration oscillation impacting the flame front. At IP_{500}, for a flame with Φ = 0.9 and a larger equivalence ratio, the LFF end does not develop into a typical tulip flame, while the flame front position does not fluctuate. The high-frequency fluctuation of velocity and the multiple finger flame fronts occur only when the equivalence ratio is 0.8. Figure 7 depicts the local amplification of the RFF. Multiple finger flame fronts occur after 46.4 ms of ignition. The right side of the picture illustrates the relative position of the flame front at each

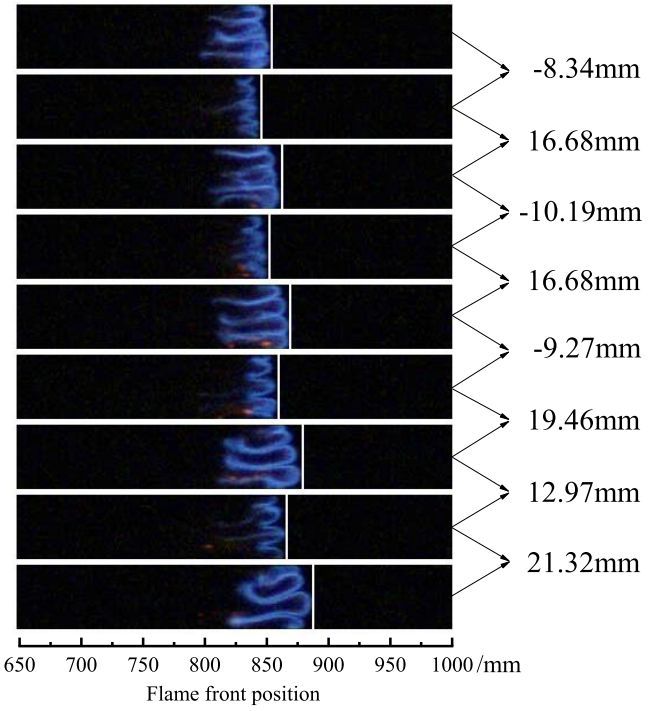

Figure 7. Pictures of multiple finger flame oscillations (ignition at IP_{500}, Φ = 0.8).

pulsation. The positive value represents the forward position of the RFF end, while the negative value denotes the backward position of the LFF end. This oscillation phenomenon of the flame in the burner is highly unfavorable to the stability of the entire combustion system.

3.3. Overpressure Dynamics. Pressure wave has a great influence on flame oscillation and flame shape change. When the ignition position is IP_0, the pressure is weakened through the closed end of the duct. When the ignition position is transferred to IP_{500}, the flame on the right side propagates to the closed end, which will inevitably undergo a complex reflection process in the duct to form a reflected pressure wave. The pressure wave is coupled with the flame so that the ignition position at IP_{500} presents a different flame shape and flame propagation law from the IP_0 position. Typical pressure signals at two different ignition positions IP_0 and IP_{500} are shown in Figure 8. When the ignition position is IP_{500}, the oscillation of the overpressure in the later stage is more obvious, and the time to reach the maximum pressure peak is shorter compared with the time to reach the maximum pressure at the ignition position IP_0. The flame structure photographs corresponding to several typical pressure points are marked with the corresponding serial numbers in the figure. In Figure 8b, when the pressure reaches the first peak A, the PVC membrane ruptures. Masri et al.[35] call this pressure peak the membrane rupture pressure or exhaust pressure. After the membrane ruptures, the gas in the duct begins to release. The overpressure drops sharply after rising for a short period. The finger-shaped flame front at the RFF end begins to flatten and is gradually dented toward the LFF end. When the pressure reaches the first trough, the flame at the LFF end was completely discharged out of the tube. At this time, the flame on the right side controls the pressure oscillation. After that, the flame undergoes a large-amplitude oscillation stage and continues to C. The process from point C to point D corresponds to the small-amplitude oscillation of the flame until it spreads to the end of the duct.

Figure 9 shows the effect of the equivalence ratio on the evolution of overpressure under different ignition positions. The maximum overpressure corresponding to each working condition and the time to reach the maximum overpressure are given separately in Figure 10. The error of repeated experiments is represented by error bars. It can be seen from the figure that when the ignition position is IP_0, the higher the equivalence ratio, the greater the maximum pressure, which is 34.9, 35.3, 36.2, 36.5, and 40.8 kPa, respectively, and the shorter the time to reach the maximum pressure, which is 16.1, 12.8, 10.8, 8.4, and 7.85 ms, respectively. Also, similar variations occur for the ignition position IP_{500}.

Figure 11a,b shows the coupling relationship between the flame propagation velocity and the overpressure when the equivalence ratio Φ = 1.0 and the ignition positions are IP_0 and IP_{500}, respectively. From Figure 11a, it can be seen that there is a strong correspondence between the flame front velocity at the IP_0 position and the overpressure. In the finger flame phase, the flame speed increases linearly until it reaches the first speed peak, after which the flame front gradually flattens to form a tulip flame, and the flame speed decreases until the first trough. When the PVC film ruptures, due to the release of gas in the duct, the overpressure begins to drop sharply, pulling the flame at the LFF end, causing the flame to accelerate to the second peak. The subsequent overpressure oscillation and

https://doi.org/10.1021/acsomega.2c01960
ACS Omega 2022, 7, 20118−20128

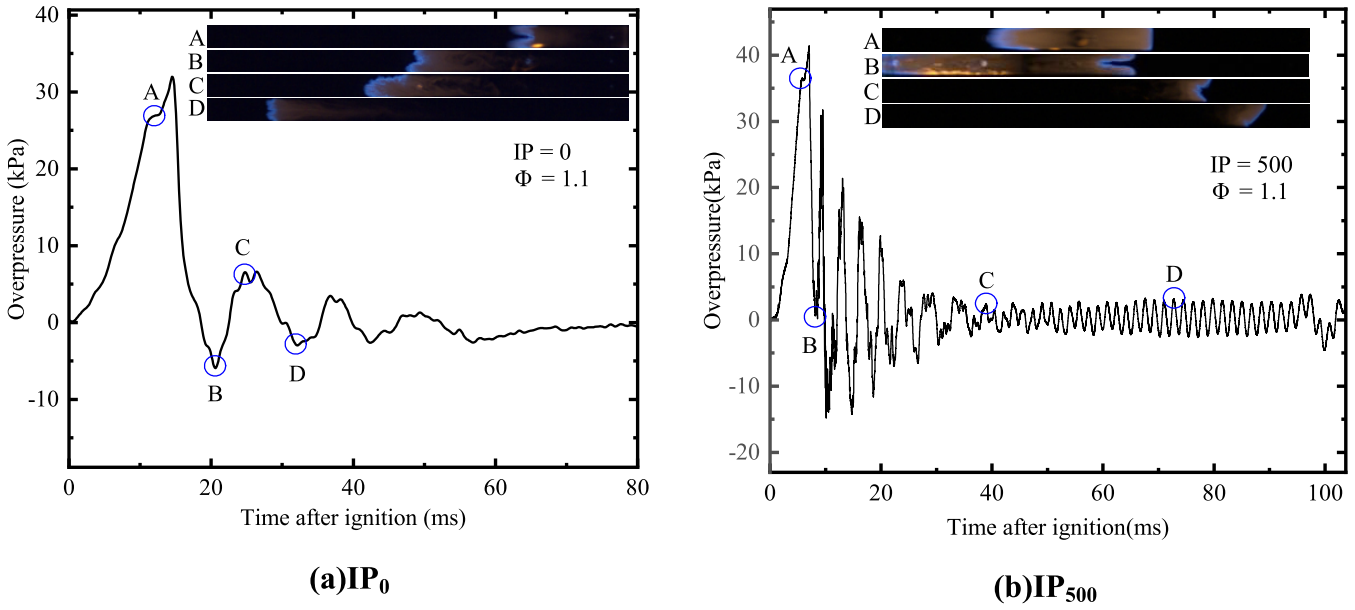

Figure 8. Coupling relationship between flame oscillation pressure and structure evolution when Φ = 1.1: (a) IP_0 and (b) IP_{500}.

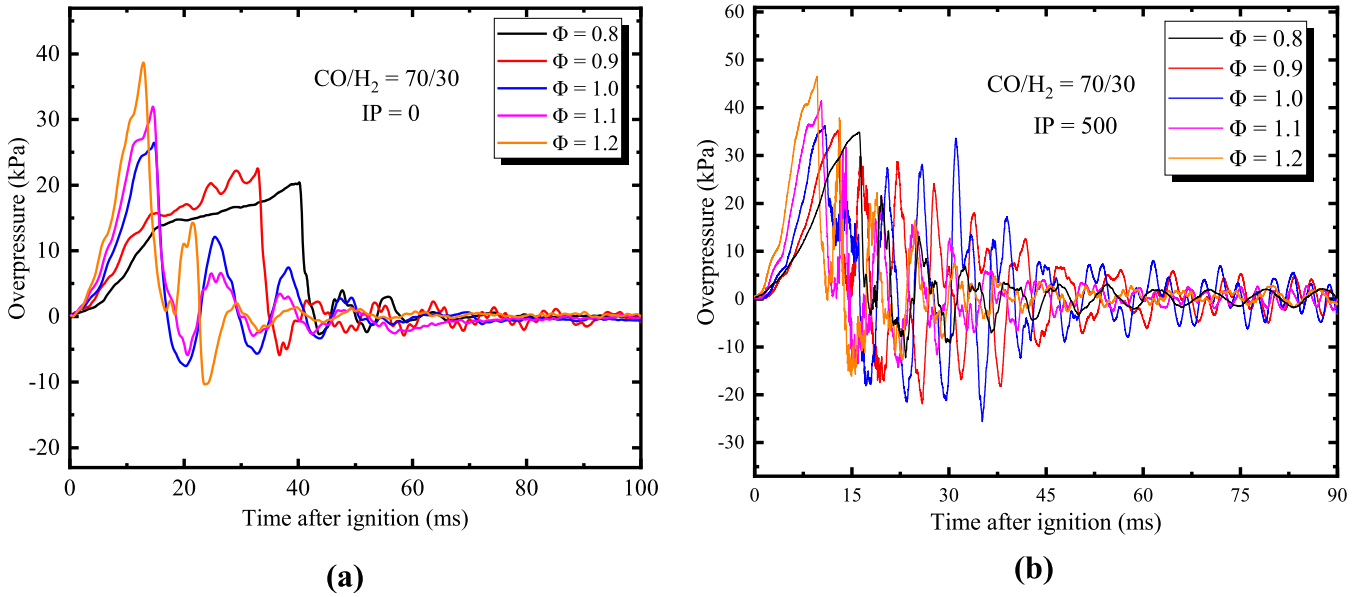

Figure 9. Time evolution of pressure: (a) IP_0 and (b) IP_{500}.

flame velocity oscillation maintain the same period and frequency.

When the ignition position is IP_{500}, the flame quickly passes from the LFF end to the outside of the tube. At this time, the change in the speed of the RFF end is mainly considered. It can be seen from Figure 11b that the flame velocity at the RFF end and the overpressure also have a good relationship. After the ignition, the flame front speed gradually increases. When the PVC film at the opening is ruptured, the flame at the RFF side is pulled in the direction of ignition due to the release of gas. The flame front begins to flatten and form a tulip flame, and the speed also decreased. After that, the pressure fluctuates up and down regularly, and it is consistent with the oscillation of the speed.

Through the analysis of the pressure data, it can be seen that when the ignition position is far away from the closed end, the overpressure oscillation becomes more severe. For different ignition positions, the pressure wave experiences different propagation processes in the duct. When the ignition position is IP_{500}, the coupling effect of the flame and the sound wave has a great impact on the overpressure oscillation. Under this influence, the syngas/air premixed gas at a specific equivalence ratio produces secondary oscillations and multiple finger-shaped flame fronts.

4. CONCLUSIONS

In this article, the explosion characteristics of syngas under different equivalence ratios and different ignition positions are studied in the Hele-Shaw duct. Syngas is composed of 30% H_2 and 70% CO. The ignition position is set at IP_0 (0 mm from the ignition point) and IP_{500} (500 mm from the ignition power). The setting range of equivalence ratio is 0.8−1.2. From the analysis of flame structure, flame tip characteristics including flame front position and speed, overpressure

https://doi.org/10.1021/acsomega.2c01960
ACS Omega 2022, 7, 20118−20128

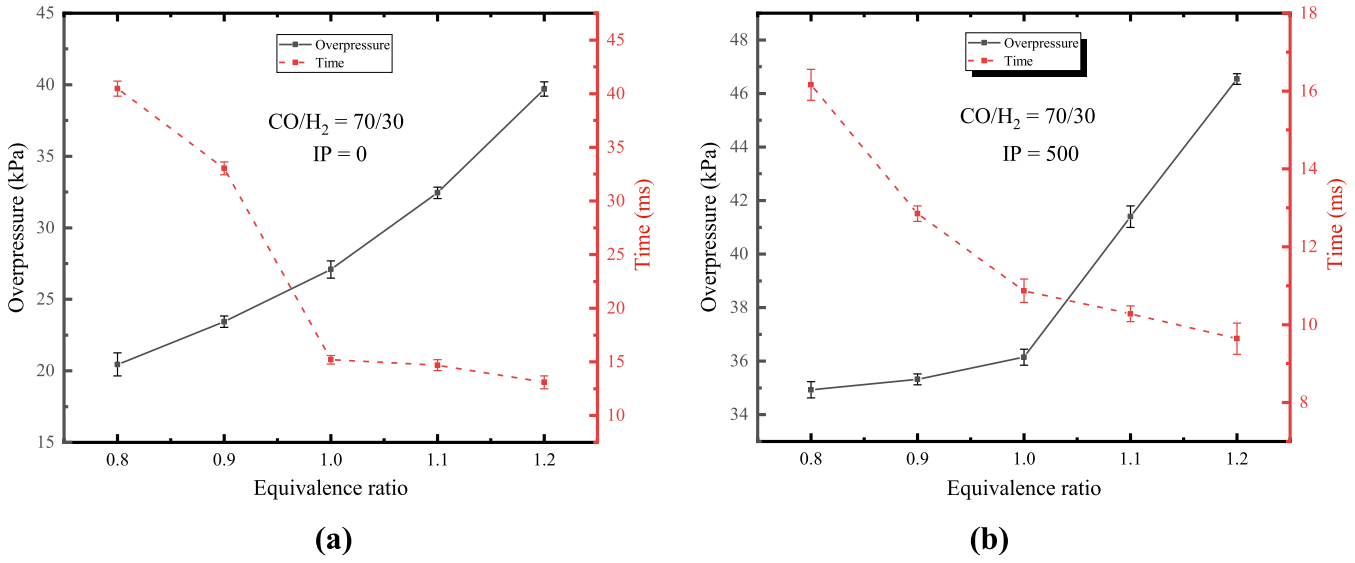

Figure 10. Maximum overpressure and arrival time under different equivalence ratios: (a) IP_0 and (b) IP_{500}.

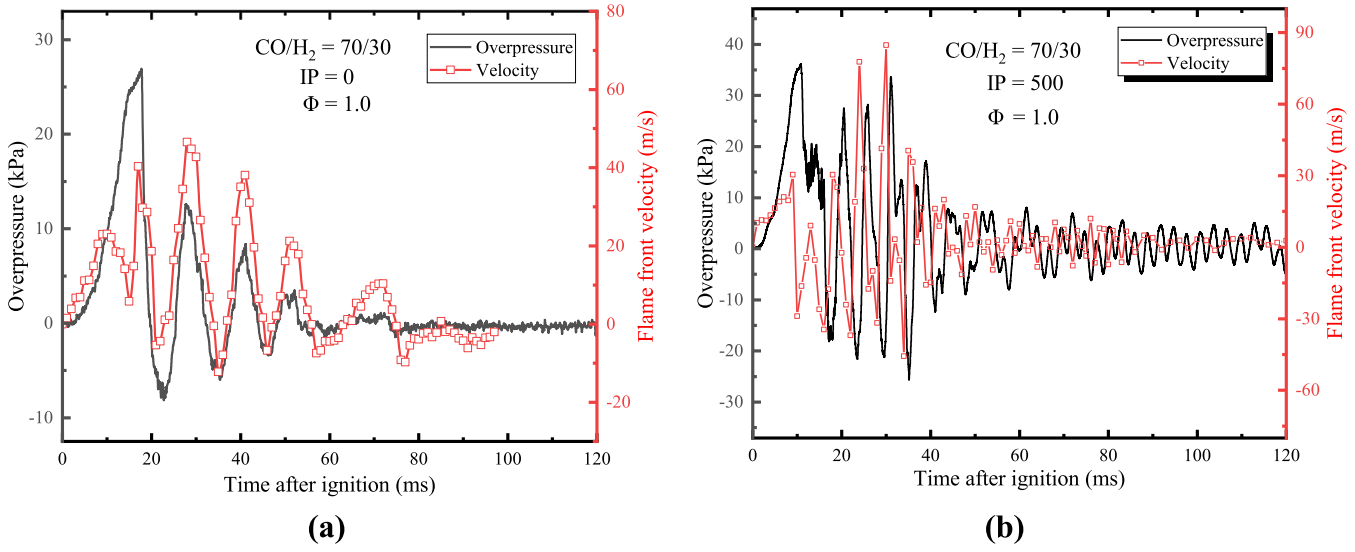

Figure 11. Curves of flame front velocity and pressure at different ignition positions: (a) IP_0 and (b) IP_{500}.

dynamics change, and other data, the following conclusions are drawn:

(1) The evolution of the flame structure in the Hele-Shaw duct is significantly influenced by different ignition positions. Ignited at IP_0, the flame spreads to the open end. Within the range of equivalence ratio studied, spherical flame, finger-shaped flame, and tulip flame appeared in all cases. When the ignition position is IP_{500} in the middle of the duct, the flame at the LFF end does not form a tulip flame. For lean-burn flames with an equivalence ratio less than 0.9, the RFF end also did not form an obvious tulip flame shape. In particular, multiple finger-like wrinkles appear when the flame front is at the ignition position of IP_{500} and the equivalence ratio is 0.8. We analyze that the Lewis number plays an important role in the occurrence of this phenomenon.

(2) The equivalence ratio has a great influence on the position and speed of the flame front. As the equivalence ratio grows at the IP_0 ignition position, the time required by the flame to travel to the end of the duct gradually reduces. The time required for the flame to spread to the LFF and RFF ends reduces as the equivalence ratio grows when the ignition position is IP_{500}.

(3) The equivalence ratio and ignition position have a great influence on the overpressure. As the ignition position moves away from the closed end (IP_{500}), the maximum pressure in the tube becomes larger and the overpressure oscillation becomes more severe. For the same ignition position, the pressure increases the rate, and the highest pressure in the tube increases with the increase in the equivalence ratio, and the time to reach the highest pressure peak gradually decreases with the increase in the equivalence ratio.

AUTHOR INFORMATION

Corresponding Author

Xiaoping Wen − *School of Mechanical and Power Engineering, Henan Polytechnic University, Jiaozuo 454003, P. R. China;* orcid.org/0000-0002-5821-5130; Email: wenxiaoping666@163.com

https://doi.org/10.1021/acsomega.2c01960
ACS Omega 2022, 7, 20118−20128

Authors

Shoutong Diao − *School of Mechanical and Power Engineering, Henan Polytechnic University, Jiaozuo 454003, P. R. China*

Zhidong Guo − *State Key Laboratory of Coal Mine Disaster Dynamics and Control, Chongqing University, Chongqing 400044, P. R. China*

Wenqiang He − *School of Mechanical and Power Engineering, Henan Polytechnic University, Jiaozuo 454003, P. R. China*

Haoxin Deng − *School of Mechanical and Power Engineering, Henan Polytechnic University, Jiaozuo 454003, P. R. China*

Fahui Wang − *School of Mechanical and Power Engineering, Henan Polytechnic University, Jiaozuo 454003, P. R. China*

Complete contact information is available at: https://pubs.acs.org/10.1021/acsomega.2c01960

Notes

The authors declare no competing financial interest.

■ ACKNOWLEDGMENTS

This paper is supported by the National Natural Science Foundation of China. (Nos. 51774115 and 52004085)

■ REFERENCES

(1) Shahbaz, M.; Yusup, S.; Inayat, A.; Patrick, D. O.; Pratama, A.; Ammar, M. Optimization of hydrogen and syngas production from PKS gasification by using coal bottom ash. *Bioresour. Technol.* **2017**, *241*, 284−295.

(2) He, D.; Yan, W. Influences of different diluents on NO emission characteristics of syngas opposed-flow flame. *Int. J. Hydrogen Energy* **2018**, *43*, 2570−2584.

(3) Pierorazio, A. J.; Baker, Q. A. Hazards for syngas fires and explosions. *Process Saf. Prog.* **2010**, *29*, 288−292.

(4) Yu, M.; Luan, P.; Zheng, K.; Yang, X.; Han, S.; Duan, Y. Experimental study on explosion characteristics of syngas with different ignition positions and hydrogen fraction. *Int. J. Hydrogen Energy* **2019**, *44*, 15553−15564.

(5) Yang, X.; Yu, M.; Zheng, K.; Wan, S.; Wang, L. A comparative investigation of premixed flame propagation behavior of syngas-air mixtures in closed and half-open ducts. *Energy* **2019**, *178*, 436−446.

(6) Guo, Z.; Wen, X.; Zhang, S.; Wang, F.; Pan, R.; Sun, Z. Experimental study on the combustion-induced rapid phase transition of syngas/air mixtures under different conditions. *Int. J. Hydrogen Energy* **2020**, *45*, 19948−19955.

(7) Yao, Z.; Deng, H.; Zhao, W.; Wen, X.; Dong, J.; Wang, F.; Chen, G.; Guo, Z. Experimental study on explosion characteristics of premixed syngas/air mixture with different ignition positions and opening ratios. *Fuel* **2020**, *279*, No. 118426.

(8) Sun, Z. Y. Laminar Explosion Properties of Syngas. *Combust. Sci. Technol.* **2020**, *192*, 166−181.

(9) Singh, D.; Nishiie, T.; Tanvir, S.; Qiao, L. An experimental and kinetic study of syngas/air combustion at elevated temperatures and the effect of water addition. *Fuel* **2012**, *94*, 448−456.

(10) Zheng, K.; Yang, X.; Yu, M.; Si, R.; Wang, L. Effect of N_2 and CO_2 on explosion behavior of syngas/air mixtures in a closed duct. *Int. J. Hydrogen Energy* **2019**, *44*, 28044−28055.

(11) Su, Y.; Luo, Z.; Wang, T.; Chen, X.; Lu, K. Effect of nitrogen on deflagration characteristics of hydrogen/methane mixture. *Int. J. Hydrogen Energy* **2022**, *47*, 9156−9168.

(12) Zhou, S.; Gao, J.; Luo, Z.; Hu, S.; Wang, L.; Wang, T. Role of ferromagnetic metal velvet and DC magnetic field on the explosion of a C_3H_8/air mixture-effect on reaction mechanism. *Energy* **2022**, *239*, No. 122218.

(13) Hele-Shaw, H. S. Flow of water. *Nature* **1898**, *58*, No. 520.

(14) Saffman, P. G.; Taylor, G. I. The penetration of a fluid into a porous medium or Hele-Shaw cell containing a more viscous liquid. *Proc. R. Soc. London, Ser. A* **1958**, *1242*, 312−329.

(15) Kuznetsov, M.; Grune, J. Experiments on combustion regimes for hydrogen/air mixtures in a thin layer geometry. *Int. J. Hydrogen Energy* **2019**, *44*, 8727−8742.

(16) Kurdyumov, V. N.; Matalon, M. Effects of gas compressibility on the dynamics of premixed flames in long narrow adiabatic channels. *Combust. Theory Modell.* **2016**, *20*, 1046−1067.

(17) Veiga López, F. *Flame Propagation in Narrow Channels*; Universidad Carlos III de Madrid, 2020.

(18) Wongwiwat, J.; Gross, J.; Ronney, P. D. Flame propagation in narrow channels at varying Lewis number *25th ICDERS*, 2015, pp 3−8.

(19) Jang, H. J.; Jang, G. M.; Kim, N. I. Unsteady propagation of premixed methane/propane flames in a mesoscale disk burner of variable-gaps. *Proc. Combust. Inst.* **2019**, *37*, 1861−1868.

(20) Jang, H. J.; Lee, S. M.; Kim, N. I. Effects of ignition disturbance on flame propagation of methane and propane in a narrow-gap-disk-burner. *Combust. Flame* **2020**, *215*, 124−133.

(21) Lee, S. M.; Jang, H. J.; Kim, N. I. Premixed flame propagation of CH_4 and C_3H_8 in a narrow-gap disk burner using constant-volume processes at elevated-pressure. *Combust. Flame* **2021**, *231*, No. 111482.

(22) Jiang, L.; Su, H.; Huo, J.; Li, X.; Yang, H.; Zhao, D. Experimental study on propane/air flame propagation characteristics in a disc-like gap chamber. *Combust. Sci. Technol.* **2019**, *191*, 1168−1183.

(23) Zhou, G.; Jiang, L.; Gu, C.; Wang, X.; Yang, W.; Zhao, D. Experimental investigation on ignition and combustion characteristics of n-butane/air mixtures by glow plug in miniature chamber. *Fuel* **2020**, *274*, No. 117857.

(24) Su, H.; Huo, J.; Wang, X.; Jiang, L.; Song, Q.; Zhao, D. Flame Propagation and Combustion State Transition in a Sub-millimeter Constant-volume Space. *Combust. Sci. Technol.* **2021**, *193*, 1866−1884.

(25) Wu, Y.; Wen, X.; Guo, Z.; Zhang, S.; Deng, H.; Wang, F. Experimental study on the propagation characteristics of hydrogen/methane/air premixed flames in a narrow channel. *Int. J. Hydrogen Energy* **2022**, *47*, 6377−6387.

(26) Diao, S.; Wen, X.; Guo, Z.; He, W.; Deng, H.; Wang, F. Experimental study of explosion dynamics of syngas flames in the narrow channel. *Int. J. Hydrogen Energy* **2022**, *47*, 17808−17820.

(27) Wen, X.; Wang, M.; Su, T.; Zhang, S.; Pan, R.; Ji, W. Suppression effects of ultrafine water mist on hydrogen/methane mixture explosion in an obstructed chamber. *Int. J. Hydrogen Energy* **2019**, *44*, 32332−32342.

(28) Salamandra, G. D.; Bazhenova, T. V.; Naboko, I. M. Formation of detonation wave during combustion of gas in combustion tube. *Symp. Int. Combust.* **1958**, *7*, 851−855.

(29) Clanet, C.; Searby, G. On the "tulip flame" phenomenon. *Combust. Flame* **1996**, *105*, 225−238.

(30) Dinkelacker, F.; Manickam, B.; Muppala, S. Modelling and simulation of lean premixed turbulent methane/hydrogen/air flames with an effective Lewis number approach. *Combust. Flame* **2011**, *158*, 1742−1749.

(31) Muppala, S.; Nakahara, M.; Aluri, N. K.; Kido, H.; Wen, J. X.; Papalexandris, M. V. Experimental and analytical investigation of the turbulent burning velocity of two-component fuel mixtures of hydrogen, methane and propane. *Int. J. Hydrogen Energy* **2009**, *34*, 9258−9265.

(32) Bouvet, N.; Halter, F.; Chauveau, C.; Yoon, Y. On the effective Lewis number formulations for lean hydrogen/hydrocarbon/air mixtures. *Int. J. Hydrogen Energy* **2013**, *38*, 5949−5960.

(33) D'Ippolito, C. *A Numerical Study of Syngas Laminar Premixed Flames: Effects of Lewis Number and Flame Stretch*; University of Illinois at Chicago, 2015.

(34) Davis, S. G.; Joshi, A. V.; Wang, H.; Egolfopoulos, F. An optimized kinetic model of H_2/CO combustion. *Proc. Combust. Inst.* **2005**, *30*, 1283−1292.
(35) Ibrahim, S. S.; Masri, A. R. The effects of obstructions on overpressure resulting from premixed flame deflagration. *J. Loss Prev. Process Ind.* **2001**, *14*, 213−221.

https://doi.org/10.1021/acsomega.2c01960
ACS Omega 2022, 7, 20118−20128